Frontiers of Information Technology & Electronic Engineering
www.jzus.zju.edu.cn; engineering.cae.cn; www.springerlink.com
ISSN 2095-9184 (print); ISSN 2095-9230 (online)
E-mail: jzus@zju.edu.cn

Ball-disk rotor gyroscope adaptive quick-start technique*

Xiao-wei LIU[1,2], Rui WENG[†‡1], Hai LI[1], Hai-feng ZHANG[1]

([1]*MEMS Center, Harbin Institute of Technology, Harbin 150001, China*)

([2]*MOE Key Laboratory of Micro-Systems and Micro-Structures Manufacturing, Harbin 150001, China*)

[†]E-mail: hit00@126.com

Received Jan. 21, 2016; Revision accepted May 1, 2016; Crosschecked Sept. 25, 2017

Abstract: Rotating speed is a critical parameter affecting the performance of rotor gyroscopes. Rotor gyroscopes must operate at the rated rotating speed. To shorten the start time of the ball-disk rotor gyroscope, this paper presents a new design of the drive system for a ball-disk rotor gyroscope. The drive system is monitored by a microcontroller. First, the microcontroller generates a sine pulse width modulation signal to drive the permanent magnet rotor. Second, the position of the rotor is detected according to the back electromotive force in the non-energized coil. Third, a piecewise closed-loop control algorithm is implemented to keep the angular acceleration of the rotor within the safe range automatically during the acceleration process and when running at a constant speed. This control algorithm can avoid rotor stalling due to loss of steps. Experimental result shows that with the help of adaptive quick-start technique, the start time of the device can be shortened by up to 36.6%.

Key words: Rotor gyroscope; Magnetically driven; Quick start; Piecewise algorithm; Closed-loop control
https://doi.org/10.1631/FITEE.1600035 **CLC number:** TN965

1 Introduction

A gyroscope is a device to measure angular motion and commonly used in many areas. Rotor gyroscopes can provide high accuracy at small size and low cost (Barbour and Schmidt, 2001; Geen, 2005; Wu *et al*., 2006a; Han *et al*., 2012). Compared to other types of gyroscope, the manufacturing of rotor gyroscopes is relatively easy. Rotor gyroscopes are generally driven by magnetic or electrostatic force (Dauwalter and Ha, 2005; Wang *et al*., 2006; Xue *et al*., 2009a; 2009b; Jin *et al*., 2011). In this paper, a miniaturized magnetically driven rotor gyroscope is discussed. While scaling down the component, the sensitivity and resolution are reduced simultaneously (Shao *et al*., 2006; Wu *et al*., 2006b). To solve this problem, the rotating speed of the rotor must be increased to a higher level. However, in the case of constant acceleration, a higher rotating speed means a longer start-up time. Therefore, the optimization of the accelerating method is an effective way to reduce the start-up time of a rotor gyroscope.

The device presented in this paper is a new design using a ball-disk rotor. The ball-disk rotor structure is based on the principles of hydrodynamic bearings, reducing the rotational resistance torque. It is possible to improve the driving efficiency while reducing the power consumption of the whole gyroscope system (Shearwood *et al*., 2000). In this structure, the ball-disk rotor is made of permanent magnetic material, and is directly driven by the coils of the stator, which is somewhat similar to the structures reported by Shearwood and Yates (1997), Damrongsak and Kraft (2005), Damrongsak *et al.* (2008), and Kraft and Damrongsak (2010). However, there are still some differences from their systems. In the ball-disk structure, the rotor and the stator are isolated by an oil film, and there is no requirement of levitation

‡ Corresponding author

* Project supported by the National Basic Research Program of China (No. 2012CB934104), the National Natural Science Foundation of China (No. 61474034), the Natural Science Foundation of Heilongjiang Province of China (No. F201418), and the Fundamental Research Funds for the Central Universities, China (Nos. HIT.NSRIF. 2014040 and HIT.NSRIF.2013040)

ORCID: Rui WENG, http://orcid.org/0000-0003-3830-7385

coils. The ball-shaped part of the rotor acts as the bearing, and the disk-shaped part acts as the main part of the mass of the gyroscope.

During the acceleration process, the driving force overcomes the resistance torque of the rotor and also provides an angular acceleration to the ball-disk rotor. If the driving torque is not sufficient, the start-up procedure of the gyroscope will fail because of the loss of steps. So, the angular acceleration must be strictly controlled within a safe range. In the original design, control of acceleration is realized by slowing down the accelerating procedure. It takes a long time to finish the start-up procedure. In this design, the system is monitored by a microcontroller unit (MCU). MCU generates a sine pulse width modulation (SPWM) driving signal and determines the angular position of the rotor, to achieve closed-loop control. The power stage amplifies the output current from MCU, and the precise amplifier makes the back-electromotive force (back-EMF) signal from the coils large enough to be picked up by the analog-to-digital converter (ADC). The adaptive quick start-up algorithm running in MCU can automatically adjust the angular acceleration during the start-up procedure. Under the control of the adaptive quick start-up algorithm, the average angular acceleration during start-up can be much larger than that of the original system, so the start-up time of the rotor gyroscope can be considerably shortened.

2 Structures and operating principle

2.1 Mechanical structures

The mechanical structure of the ball-disk rotor gyroscope is illustrated in Fig. 1.

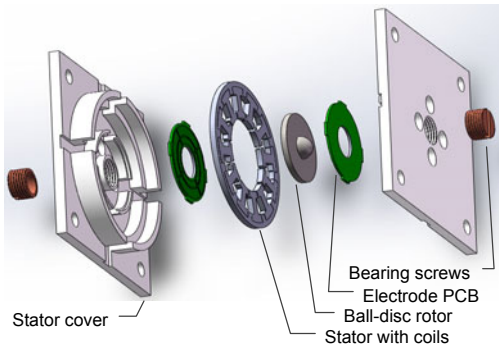

Fig. 1 Structure of the ball-disk rotor gyroscope

The ball-disk rotor is composed of a magnetic steel sheet and a precision steel ball, the stator iron core is made of stacked silicon steel sheets, while the stator covers and bearing screws are made of beryllium copper. All the parts mentioned above are prepared by precision CNC turning, milling, and wire-cutting processes. It can be observed in Fig. 1 that the ball-disk rotor is assembled at the center of the structure, with the stator iron core surrounded by 12 coils. There are two sets of detection PCB electrodes installed in parallel to the disk structure of the rotor. The ball-disk rotor constitutes the mass in the gyroscope system. When the system works, the rotating magnetic field generated by the coils makes the ball-disk rotor rotate. If there is an external angular velocity input to the system, the rotor deflects because of the Coriolis force. The deflection changes the differential capacitance between the rotor and the PCB electrodes. Then the input signal is detected by the system.

2.2 Operating principle

With the rotor center as the origin, we establish a Cartesian coordinate system $Oxyz$. The disk is parallel to the plane xOy, and the rotor rotates around the z axis (Fig. 2).

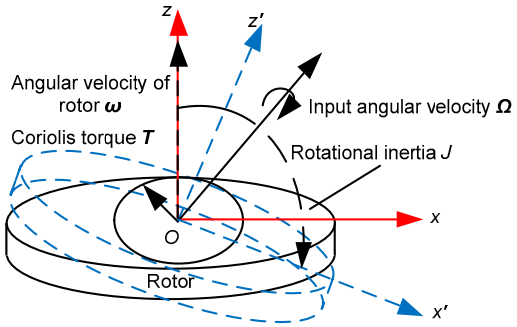

Fig. 2 Precession of the ball-disk rotor

Considering the ball-disk rotor as a homogeneous, ideal rigid body, the relationship among Coriolis torque $\boldsymbol{T}$, input angular velocity $\boldsymbol{\Omega}$, rotational inertia J, and the rotor's angular velocity $\boldsymbol{\omega}$ can be described by the following formula:

$$\boldsymbol{T} = J\boldsymbol{\omega} \times \boldsymbol{\Omega}. \tag{1}$$

For a ball-disk rotor with density ρ, its rotational inertia can be described as

$$J=\iiint r^2\rho \mathrm{d}V. \tag{2}$$

Then, the value of the Coriolis torque can be described as

$$T=\iiint r^2\rho \mathrm{d}V\cdot\omega\Omega. \tag{3}$$

Fig. 3 shows the angle φ between the rotor's disk plane and the stator plane.

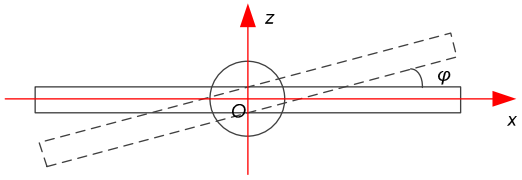

Fig. 3 Diagram of rotor deflection

When φ is very small, the sub-torque T_s of the electromagnetic drive torque can be deduced approximately as

$$T_s=T_{drive}\sin\varphi, \tag{4}$$

where T_{drive} is the electromagnetic drive torque. When Coriolis torque T_c is equal to sub-torque T_s in the opposite direction, the system reaches balance status. Thus, input angular velocity $\boldsymbol{\Omega}$ can be deduced by detecting angle φ.

3 Driving method and position detection

3.1 Driving method

The plan view of the ball-disk gyroscope is shown in Fig. 4. As can be seen, the stator coils are divided into 12 poles. A pole is a region where the magnetic flux density is concentrated. A pair of poles in the radial direction of the rotor constitutes one phase. There are six phases in the system: *A*, *B*, *C*, *D*, *E*, and *F*.

Taking phase *A* for detailed analysis, when this phase is energized, the rotor will rotate counterclockwise to keep the magnetic circuit shortest. The magnetic torque $\boldsymbol{M}$ that drives the rotor can be expressed as

$$\boldsymbol{M}=\boldsymbol{P}\times\boldsymbol{B}, \tag{5}$$

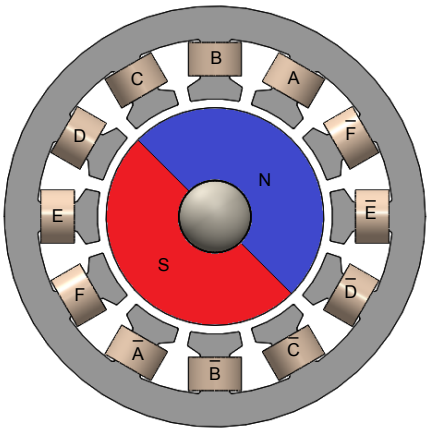

Fig. 4 Plan view of the ball-disk gyroscope

where $\boldsymbol{P}$ is the composition of magnetic moments of energized coils, and $\boldsymbol{B}$ is the magnetic flux density of the ball-disk rotor. Because of the difference between the magnetized rotors, flux density $\boldsymbol{B}$ cannot be accurately determined. That is to say, the value of $\boldsymbol{B}$ can be obtained only by experiments.

Compared to the rectangular wave driving method, the symmetrical SPWM signal can drive the device more smoothly (Srinu and Manmadha, 2014; Xu *et al*., 2014). In this system, the six-phase SPWM driving signal is used to energize the driving coils. The phase difference between two adjacent phases is 60°. The waveform of each phase is shown in Fig. 5.

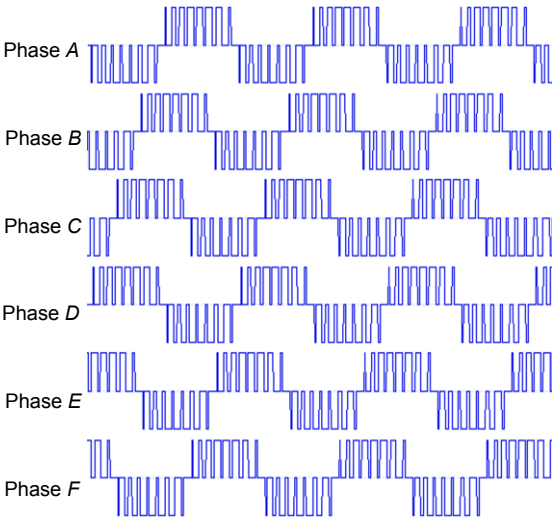

Fig. 5 Driving waveform of each phase

The ball-disk rotor gyroscope driving system is monitored by an MCU. MCU picks up the back-EMF signal during the silent period of SPWM signal to determine the position of the rotor. Under the control of MCU, the ball-disk rotor can be accelerated and kept rotating at the preset speed. In addition, MCU provides a simple user interface to modify the parameters and check the status of the driving system.

3.2 Rotatory position detection

When the permanent magnet ball-disk rotor rotates, the value of magnetic flux density B_R generated in the stator core can be expressed as

$$B_R = B_m \cdot \cos(\omega t + \varphi_0), \tag{6}$$

where B_m is the maximum value of the magnetic flux density, ω is the angular speed of the ball-disk rotor, and φ_0 is the initial phase when the rotor starts to rotate. According to Faraday's law of electromagnetic induction, the electromotive force induced in the coil can be calculated by

$$E = N \cdot \frac{\mathrm{d}\varphi}{\mathrm{d}t} = N \cdot \frac{\mathrm{d}(\boldsymbol{B}_R \cdot \boldsymbol{S})}{\mathrm{d}t}, \tag{7}$$

where N is the number of turns of the coil, φ is the magnetic flux through the coil's cross section, $\boldsymbol{B}_R$ is the magnetic flux density through the cross section of the coil, and $\boldsymbol{S}$ is the cross-sectional area of the coil.

Ignoring the effects of magnetic flux leakage, the rotor's magnetic field goes through the high magnetic permeability stator cores. $\boldsymbol{B}_R$ and $\boldsymbol{S}$ in Eq. (7) are orthogonal, so we obtain

$$\boldsymbol{B}_R \cdot \boldsymbol{S} = B_R \cdot S. \tag{8}$$

Thus, Eq. (7) can be rewritten as

$$E = N \cdot \frac{\mathrm{d}(B_R \cdot S)}{\mathrm{d}t} = N \cdot \frac{S \cdot \mathrm{d}B_R + B_R \cdot \mathrm{d}S}{\mathrm{d}t}. \tag{9}$$

The size of the coil is fixed. That is, $\mathrm{d}S$=0. Substituting Eq. (6) into Eq. (9), we obtain

$$\begin{aligned} E &= N \cdot \frac{S \cdot \mathrm{d}B_R}{\mathrm{d}t} = NS \cdot \frac{\mathrm{d}[B_m \cdot \cos(\omega t + \varphi_0)]}{\mathrm{d}t} \\ &= -NSB_m\omega \cdot \sin(\omega t + \varphi_0). \end{aligned} \tag{10}$$

In this system, there is no separate back-EMF detection coil. The back-EMF signal is obtained by measuring the terminal voltage of the driving coils during the non-driving period. In other periods, the values are copied from the last valid sample. Fig. 6 shows the waveforms of the ideal drive signal, the terminal voltage of the coil, and the sampled back-EMF signal.

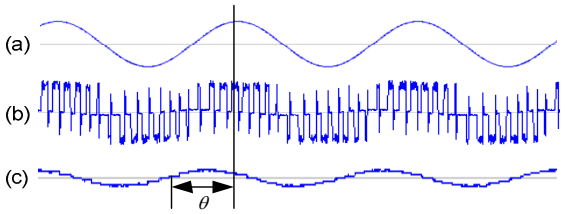

Fig. 6 Ideal drive signal (a), terminal voltage waveform (b), and sampled back-EMF signal (c)
θ is the angle between the ideal drive signal and back-EMF signal

According to Eq. (10), the zero-crossing point of the back-EMF signal occurs exactly at the position where the change rate of the magnetic flux density is zero. That is just when one of the rotor's magnetic poles passes the detection coil. Considering the slope of the induced back-EMF signal, the rotational position of the rotor can be determined.

4 Modeling and simulation

During the accelerating procedure, the driving torque not only overcomes the resistance torque between the rotor and the stator, but also provides the angular acceleration of the rotor. When the driving signal increases, the angle between $\boldsymbol{B}$ and $\boldsymbol{P}$ will increase to provide angular acceleration to the rotor. However, when the angle is greater than a certain value, the rotor cannot keep pace with the rotating speed of the magnetic field. The angle continues to increase, and when the angle is greater than 180°, the direction of the driving torque is reversed and the rotor stalls. In this case, the rotor will never spin up again on its own, causing failure of the start of the system.

In an actual system, the maximum driving power is limited, and it can be described as

$$P = (\boldsymbol{T}_{res} + J\boldsymbol{\alpha}) \cdot \boldsymbol{\omega} \le P_{max}, \tag{11}$$

where P is the actual output power of the driving system, $\boldsymbol{T}_{\mathrm{res}}$ is the resistance torque, J is the rotational inertia of the rotor, $\boldsymbol{\alpha}$ is the angular acceleration of the rotor, $\boldsymbol{\omega}$ is the angular velocity of the rotor, and $P_{\max}$ represents the maximum drive power.

The rotational inertia of the ball-disk rotor used in this system can be calculated according to the mechanical dimensions and the material properties. The result is

$$J \approx 5.11\times10^{-8}\ \mathrm{kg\cdot m^2}. \tag{12}$$

The system described here is powered up by a 5 V power supply, and the input current limit is 1 A. The power consumption of MCU is about 200 mW, so the maximum drive power is calculated as

$$P_{\max} \approx UI_{\max} - P_{\mathrm{MCU}} = 4.8\ \mathrm{W}. \tag{13}$$

To ensure system reliability, some power margin is set here. Take P_{limit}=4.5 W as the maximum driving power in this system.

At a low rotating speed, the back-EMF signal is too weak to complete zero-crossing detection. The closed-loop control will not be able to operate until the rotating speed reaches 2000 r/min. Thus, the start-up process requires a separate treatment.

When the rotor begins to spin up from standstill, the oil film does not exist between the rotor ball and the bearing screws, and the resistance torque is relatively large. When the rotating speed becomes higher, the oil film forms, and then the resistance torque reduces significantly and increases slowly with the increase of the rotating speed (Deng *et al*., 2011).

In Eq. (11), let $\boldsymbol{\alpha}$=**0** (i.e., steady state). $\boldsymbol{T}_{\mathrm{res}}$ can be deduced approximately by measuring the minimum steady-state driving power $P_{\mathrm{min(steady)}}$ and the angular speed $\boldsymbol{\omega}$. Experiments show that the resistance torque variation is very small, and $\boldsymbol{T}_{\mathrm{res}}$ can be considered a constant:

$$T_{\mathrm{res}} \approx 2.07\times10^{-2}\ \mathrm{N\cdot m}. \tag{14}$$

Through numerical simulations, the system characteristics can be predicted quickly (Xiao *et al*., 2010; Qin *et al*., 2011; Shao *et al*., 2011). Fig. 7 shows the piecewise control algorithm of the gyroscope driving system. To evaluate the performance of the system, an equivalent simulation model of this system was built with SIMULINK.

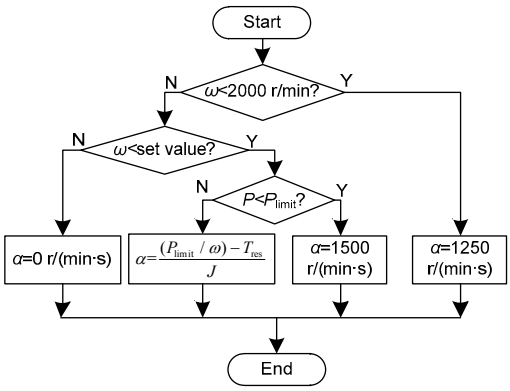

Fig. 7 Control algorithm of the gyro driving system

The algorithm can be described as follows: at the beginning, the rotating speed is below 2000 r/min, and it is accelerated with the initial angular acceleration of 1250 r/(min·s). When the rotating speed just reaches 2000 r/min, the angular acceleration increases to 1500 r/(min·s). As the speed increases further, the maximum driving power P_{limit} will limit the angular acceleration. At this time, the alternative value limited by P_{limit} will be used. The angular acceleration gradually decreases with increasing speed. When the rotating speed reaches the set value of 8700 r/min, the system completes the start-up procedure.

Throughout the above process, as long as the back-EMF detection system can work, the lag angle θ in Fig. 6 can be monitored. If θ>80°, the angular acceleration is forced to be zero until θ returns to the safe range. This can ensure that the driving torque is in the correct direction to avoid loss of steps.

5 Results and discussion

Before establishing the system, an open-loop control method is used. It changes the angular acceleration according to the speed range of the rotor (Table 1).

The simulation results of the traditional open-loop method and the closed-loop driving method proposed in this study are both presented in Fig. 8. As can be seen, the open-loop system is conservative. The capability of the power supply cannot be fully used, and it takes 13.4 s to start, while the closed-loop driving method takes full advantage of the power supply and needs only 8.7 s.

Table 1 Relationship between the angular acceleration and speed range

Speed range (r/min)	Angular acceleration (r/(min·s))
[0, 2000)	1250
[2000, 4000)	893
[4000, 6000)	625
[6000, 8000)	450
[8000, max)	333

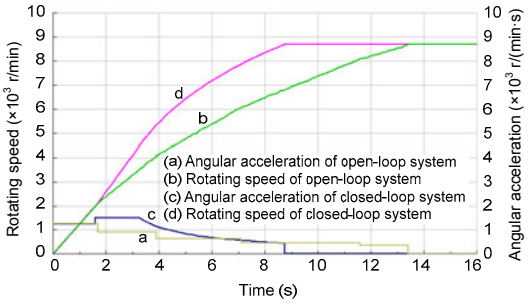

Fig. 8 Comparison between the open- and closed-loop systems

When the open- and closed-loop driving methods are applied to the same gyroscope, the start-up time can be compared. The results show that the closed-loop driving system can accelerate the rotor from standstill to 8700 r/min in around 8.7 s, while the open-loop system takes up to 13.4 s. The measured results agree with the simulation results.

During the start-up procedure, the peak-to-peak value of the back-EMF and the measured lag angle between the ideal drive signal and the back-EMF signal are as shown in Fig. 9.

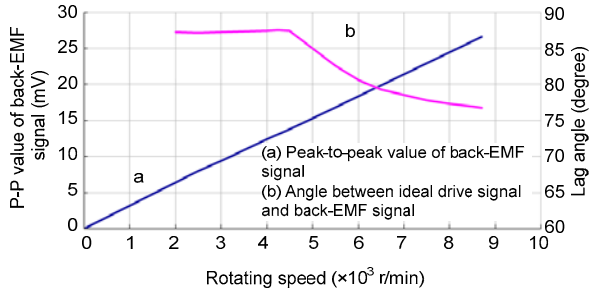

Fig. 9 Back-EMF signal and rotor speed

When the rotating speed is above 2000 r/min, the back-EMF signal is strong enough to achieve reliable zero-crossing detection. It can be seen from Fig. 8 that the lag angle is below 90° during the whole start-up procedure. The closed-loop driving system is working properly.

6 Conclusions

In this paper, a novel adaptive quick-start technique with back-EMF rotor position detection has been presented. In this technique, angular acceleration is controlled according to not only the power consumption of the system but also the relative position of the rotor. The position is detected without a separate back-EMF detection coil. This means the technology can be applied to almost all gyroscope drive systems without any necessity for modifying the coil structure. The back-EMF rotor position detection part can measure the lag angle between the ideal drive signal and the back-EMF signal and control it within the safe range, thereby avoiding loss of steps. Using the new start-up technology, the rotor of the ball-disk rotor gyroscope can be accelerated from standstill to 8700 r/min within 8.7 s, while the old open-loop startup method takes 13.4 s. The start time is shortened by 36.6%.

References

Barbour, N., Schmidt, G., 2001. Inertial sensor technology trends. *IEEE. Sens. J.*, **1**(2):332-339. https://doi.org/10.1109/7361.983473

Damrongsak, B., Kraft, M., 2005. A micromachined electrostatically suspended gyroscope with digital force feedback. IEEE Sensors, p.401-404. https://doi.org/10.1109/ICSENS.2005.1597720

Damrongsak, B., Kraft, M., Rajgopal, S., *et al.*, 2008. Design and fabrication of a micromachined electrostatically suspended gyroscope. *J. Mech. Eng.*, **222**(1):53-63. https://doi.org/10.1243/09544062JMES665

Dauwalter, C.R., Ha, J.C., 2005. Magnetically suspended MEMS spinning wheel gyro. *IEEE Aerosp. Electron. Syst. Mag.*, **20**(2):21-26. https://doi.org/10.1109/MAES.2005.1397145

Deng, S., Li, X.L., Wang, J.G., *et al.*, 2011. Frictional torque characteristic of angular contact ball bearings. *J. Mech. Eng.*, **47**(5):114-120. https://doi.org/10.3901/JME.2011.05.114

Geen, J.A., 2005. Very low cost gyroscopes. IEEE Sensors, p.537-540. https://doi.org/10.1109/ICSENS.2005.1597754

Han, F.T., Liu, Y.F., Wang, L., *et al.*, 2012. Micromachined electrostatically suspended gyroscope with a spinning

ring-shaped rotor. *J. Micromech. Microeng.*, **22**(10):1-9. https://doi.org/10.1088/0960-1317/22/10/105032

Jin, L.C., Zhang, H.W., Zhong, Z.Y., 2011. Design of a LC-tuned magnetically suspended rotating gyroscope. *J. Appl. Phys.*, **109**:07E525. https://doi.org/10.1063/1.3562263

Kraft, M., Damrongsak, B., 2010. Micromachined gyroscopes based on a rotating mechanically unconstrained proof mass. IEEE Sensors, p.23-28. https://doi.org/10.1109/ICSENS.2010.5690984

Qin, K., Zhang, W.P., Chen, W.Y., *et al*., 2011. Simulation of electrostatically suspended micro-gyroscope based on LabVIEW. 3rd Int. Conf. on Measuring Technology and Mechatronics Automation, p.249-252. https://doi.org/10.1109/ICMTMA.2011.633

Shao, D.D., Chen, W.Y., Zhang, W.P., *et al*., 2011. Virtual prototyping simulation for electrostatically suspended rotor micro gyroscope initial levitation. 6th IEEE Int. Conf. on Nano/Micro Engineered and Molecular Systems, p.9-12. https://doi.org/10.1109/NEMS.2011. 6017282

Shao, S.Y., Huang, X.G., Liu, W., *et al.*, 2006. Design of drive circuit for rotation of micromachined gyroscope with magnetic-suspension rotor. *Transd. Microsyst. Technol.*, **2**:83-85 (in Chinese).

Shearwood, C., Yates, R.B., 1997. Development of an electromagnetic micro-generator. *Electron. Lett.*, **33**(22):1883-1884. https://doi.org/10.1049/el:19971262

Shearwood, C., Ho, K.Y., Williams, C.B., *et al*., 2000. Development of a levitated micromotor for application as a gyroscope. *Sensor Actuat. A*, **83**(1-3):85-92. https://doi.org/10.1016/S0924-4247(00)00292-2

Srinu, D., Manmadha, K.B., 2014. A single phase to three phase PFC half-bridge converter using BLDC drive with SPWM technique. *Int. J. Eng. Res. Appl.*, **4**(7):31-38.

Wang, C.C., Yao, Y.D., Liu, C.S., *et al.*, 2006. Micro-magnetic suspension motor design for miniature optical drive. *Jpn. J. Appl. Phys.*, **45**(7):5801-5803. https://doi.org/10.1364/ISOM_ODS.2005.MP1

Wu, X.S., Chen, W.Y., Zhao, X.L., *et al.*, 2006a. Development of a micromachined rotating gyroscope with electromagnetically levitated rotor. *J. Micromech. Microeng.*, **16**(10):1993-1999. https://doi.org/10.1088/0960-1317/16/10/011

Wu, X.S., Chen, W.Y., Zhao, X.L., *et al.*, 2006b. Micromachined rotating gyroscope with electromagnetically levitated rotor. *Electron. Lett.*, **42**(16):912-913. https://doi.org/10. 1049/el:20061479

Xiao, Q.J., Chen, W.Y., Li, S.Y., *et al*., 2010. Modeling and simulation of levitation control for a micromachined electrostatically suspended gyroscope. *Microsyst. Technol.*, **16**:357-366. https://doi.org/10.1007/s00542-009-0927-x

Xu, J.B., Wu, Z.Z., Wu, X., *et al*., 2014. An improved phase disposition SPWM strategy for cascaded multilevel inverter. *Math. Probl. Eng.*, Article 731574. https://doi.org/10.1155/2014/731574

Xue, G., Li, T., Zhang, H.W., 2009a. Research status and development of magnetically suspended rotorgyroscopes. Int. Conf. on Applied Superconductivity and Electromagnetic Devices, p.373-376. https://doi.org/10.1109/ASEMD.2009.5306617

Xue, G., Zhang, X.T., Zhang, H.W., 2009b. Electromagnetic design of a magnetically suspended gyroscope prototype. IEEE Int. Conf. on Applied Superconductivity and Electromagnetic Devices, p.369-372. https://doi.org/10.1109/ASEMD.2009.5306616